Available online at www.sciencedirect.com
ScienceDirect
Journal of Sound and Vibration 323 (2009) 594–608
JOURNAL OF SOUND AND VIBRATION
www.elsevier.com/locate/jsvi

Theoretical modelling and effectiveness study of rail vibration absorber for noise control

H.P. Liu, T.X. Wu*, Z.G. Li

State Key Laboratory of Mechanical System and Vibration, Shanghai Jiao Tong University, Shanghai 200240, PR China

Received 28 October 2008; received in revised form 12 January 2009; accepted 18 January 2009
Handling Editor: L.G. Tham
Available online 25 February 2009

Abstract

An effective way to reduce noise from railway track is using a rail vibration absorber. A compound track–absorber model is developed to study the effectiveness of the rail absorber and the influences of its bending modes. In the model the rail absorber is represented by a damped beam–spring system attached to the rail. The calculation results show that the decay rate of rail vibration along the track is significantly increased around the tuned frequency of the absorber and thus the rail vibration energy is substantially reduced in the corresponding frequency region. In addition, the pinned–pinned resonance of track vibration is suppressed by the rail absorber. The results also show that it is the rigid body motion of the beams of the absorber that leads to energy dissipation of rail vibration, whereas the bending deformation of the beams is a minor factor. Therefore, a simple mass–spring model is enough to represent the rail absorber instead of an advanced beam–spring model.

1. Introduction

Railway induced vibration and noise are a growing matter of environmental concern. The main source of noise from the railway is rolling noise. The combined roughness on the wheel and rail tread causes vibration and radiation of the wheel, rail and sleeper.

Calculation models have been developed for understanding the mechanism of railway vibration and noise generation [1–5]. The vibration responses of the wheel, rail and sleeper contribute to the overall spectrum of noise. Amongst them, the rail is a dominant source in the frequency region 500–2000 Hz when the running speed of a train is medium, from 100 to 160 km/h.

Various measures have been taken to reduce railway rolling noise. A promising means reducing rail radiation is using a rail damper/absorber to increase the decay rate of vibration along the rail. Field tests showed that the rail radiated noise could be decreased by up to 6 dB using a tuned rail damping device, the rail absorber [6]. A combined model of the railway track with the rail absorber, which is treated as a two-degree-of-freedom mass–spring system, was developed by Wu [7] for the track dynamics with the absorber.

*Corresponding author. Tel.: +86 21 3420 6332x819; fax: +86 21 3420 5875.
E-mail address: txwu@sjtu.edu.cn (T.X. Wu).

0022-460X/$ - see front matter © 2009 Elsevier Ltd. All rights reserved.
doi:10.1016/j.jsv.2009.01.036

The mechanism of vibration energy dissipation by the rail absorber was studied in Ref. [7] and the optimal parameters and installation position for the rail absorber were determined after extensive investigation of their influences on the vibration decay rate along the track.

The models developed so far have treated the rail absorber as a mass–spring system. The simpler mass–spring model is directly applicable for some types of rail damper available on the market. For beam-like rail absorbers, however, the mass-bar in the absorber is actually a beam instead of a mass. It is not clear whether or not the bending modes of the mass-bar affect the performance of the rail absorber. Therefore, an advanced model for the rail absorber is needed, in which the bending modes of the mass-bar should be considered in order to study their effects on the performance of the rail absorber.

The main purpose of this study is to investigate the influences of the bending modes of the rail absorber on the track dynamics and performance of the absorber. First, a compound track–absorber model is developed, in which the rail is modelled as an infinite Timoshenko beam and the absorber is represented by a damped double-beam system attached to the rail via elastomeric materials. Then using this model the effects of the bending modes on the performance of the rail absorber are investigated in terms of the receptance, decay rate and energy of rail vibration, compared with those from the mass–spring model of the rail absorber. Further, as the natural frequencies and bending modes of the absorber are associated with its length and cross-section parameters, their influences are also studied.

To estimate the effectiveness of rail absorber on noise reduction, the radiation ratio of rail vibration with the absorber applied must be known, but it is not available for the time being. Nevertheless, the effectiveness can be estimated indirectly via the rail vibration energy reduced by the absorber, as the rail radiation is proportional to the mean-squared velocity of rail vibration.

2. Track model with rail absorber

Fig. 1 shows the cross-section of the rail with the absorber, which consists of the steel mass-bars and the elastomeric material layers between the mass-bars and rail. The rail absorber can be modelled as a two-degree-of-freedom mass–spring system when the mass-bar is short [7], but a beam–spring model is more appropriate if the mass-bar is long.

Only half a track is considered in the model due to symmetry as shown in Fig. 2. The track–absorber model is divided into two parts: the upper parts represent the rail absorbers and the lower parts represent the rail and its supports. The rail is modelled as an infinite Timoshenko beam, and the rail supports are discrete and composed of the rail pad, sleeper and ballast. The absorber model includes two finite Euler–Bernoulli beams with free–free boundaries, and the beams are connected by discrete springs K_1, K_2 and K_3. They are complex stiffness with loss factor η_a and at the same place along the rail with span distance d. K_1, K_2 and K_3 are treated to be discrete so that they are easily dealt with in the modelling and calculation. For the track model K_p, m_s

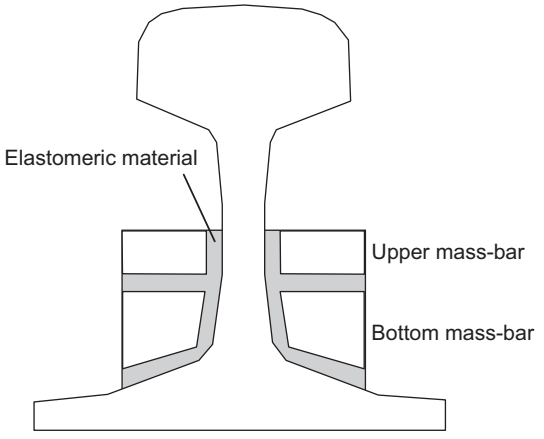

Fig. 1. Cross-section of the rail with absorber [6].

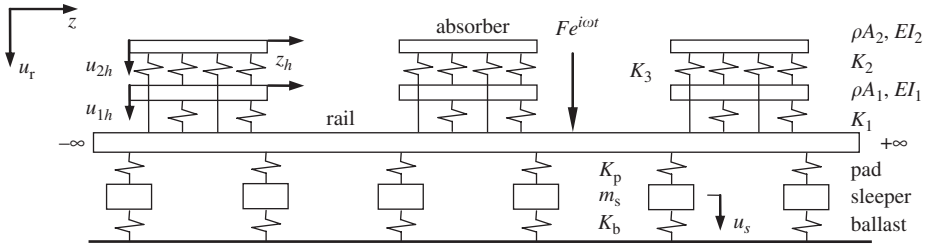

Fig. 2. Compound track–absorber model.

and K_b represent the pad stiffness, sleeper mass and ballast stiffness, respectively. K_p and K_b are also complex stiffness with loss factor η_p and η_b, respectively. D is the sleeper span length.

The material properties of the model are represented by G, the shear modulus, E, Young's modulus, and ρ, the density. The geometric properties of the beams are characterized by A, the cross-sectional area, I, the area moment of inertia and κ, the shear coefficient. The equations of motion for the rail are

$$\rho A_r \frac{\partial^2 u_r}{\partial t^2} - GA_r\kappa\left(\frac{\partial^2 u_r}{\partial z^2} - \frac{\partial \varphi}{\partial z}\right) + \sum_{n=1}^{N} K_p(u_r - u_{sn})\delta(z - z_{pn}) + \sum_{m=1}^{M}[K_1(u_r - u_{1h}) + K_3(u_r - u_{2h})]\delta(z - z_m) = f(t)\delta(z), \tag{1}$$

$$\rho I_r \frac{\partial^2 \varphi}{\partial t^2} - EI_r \frac{\partial^2 \varphi}{\partial z^2} - GA_r\kappa\left(\frac{\partial u_r}{\partial z} - \varphi\right) = 0, \tag{2}$$

where u_r is the vertical displacement and z is the longitudinal coordinates of the rail, φ is the rotation angle of the cross-section. u_{sn} represents the vertical displacement of the nth sleeper, and u_{1h}, u_{2h} are the displacement of the bottom and upper beam of the hth absorber, respectively. $K_p(u_r - u_{sn})$ is the restoring force of the nth rail pad, z_{pn} represents its position, and δ is the Dirac delta function. $K_1(u_r - u_{1h})$ and $K_3(u_r - u_{2h})$ are the restoring forces between the rail and bottom mass-bar and between the rail and upper mass-bar, respectively, and z_m represents their position. N is the number of the rail pads considered in the model and, $M = M_a \times M_p$, where M_a is the number of the absorber considered in the model and M_p is the number of the spring between the rail and mass-bar for each absorber.

The equation of motion of the bottom mass-bar of the hth absorber is given by

$$\rho A_1 \frac{\partial^2 u_{1h}}{\partial t^2} + EI_1 \frac{\partial^4 u_{1h}}{\partial z_h^4} + \sum_{j=1}^{M_p}[K_1(u_{1h} - u_r) + K_2(u_{1h} - u_{2h})]\delta(z_h - z_{hj}) = 0,$$
$$j = 1, 2, \ldots, M_p, \quad h = 1, 2, \ldots, M_a, \tag{3}$$

where z_h is the local coordinates of the hth absorber, $K_1(u_{1h} - u_r)$ and $K_2(u_{1h} - u_{2h})$ are the restoring forces to the bottom mass-bar, and z_{hj} represents their longitudinal position in the local coordinates.

The equation of motion for the upper mass-bar of the hth absorber is given by

$$\rho A_2 \frac{\partial^2 u_{2h}}{\partial t^2} + EI_2 \frac{\partial^4 u_{2h}}{\partial z_h^4} + \sum_{j=1}^{M_p}[K_2(u_{2h} - u_{1h}) + K_3(u_{2h} - u_r)]\delta(z_h - z_{hj}) = 0,$$
$$j = 1, 2, \ldots, M_p, \quad h = 1, 2, \ldots, M_a, \tag{4}$$

where $K_2(u_{2h} - u_{1h})$ and $K_3(u_{2h} - u_r)$ are restoring forces to the upper mass-bar of the hth absorber.

The equation of motion for the nth sleeper is given by

$$m_s \frac{d^2 u_{sn}}{dt^2} + K_p[u_{sn} - u_r(z_{pn})] + K_b u_{sn} = 0, \quad n = 1, 2, \ldots, N. \tag{5}$$

Assuming that the excitation and response are harmonic, then the sleeper displacement amplitude, U_{sn}, can be represented by the rail displacement amplitude, $U_r(z_{pn})$, according to Eq. (5), given as

$$U_{sn} = \frac{K_p}{K_p - m_s\omega^2 + K_b} U_r(z_{pn}), \quad n = 1, 2, \ldots, N. \tag{6}$$

Using the concept of the structure receptance and the superposition principle, the displacement of the rail and the absorber can be written as

$$U_r(z) = F\alpha(z, 0) - \sum_{n=1}^{N} F_{pn}\alpha(z, z_{pn}) - \sum_{m=1}^{M}(F_{1m} + F_{3m})\alpha(z, z_m), \tag{7}$$

$$U_{1h}(z_h) = -\sum_{j=1}^{M_p}(F_{1hj} - F_{2hj})\beta_1(z_h, z_{hj}), \quad h = 1, 2, \ldots, M_a, \tag{8}$$

$$U_{2h}(z_h) = -\sum_{j=1}^{M_p}(F_{2hj} + F_{3hj})\beta_2(z_h, z_{hj}), \quad h = 1, 2, \ldots, M_a, \tag{9}$$

where $\alpha(z, z_1)$ is the rail receptance defined as the displacement response at z caused by a unit harmonic force at z_1. $\beta_1(z, z_1)$ and $\beta_2(z, z_1)$ are the receptance of the bottom and upper mass-bar of the absorber, respectively, and they are similarly defined as the rail receptance. The rail receptance is calculated using the infinite Timoshenko beam model, and the receptance of the mass-bars is calculated using the finite Euler beam model with free–free boundary conditions. Calculation details are referred to Ref. [7] for the infinite Timoshenko beam and to Appendix for the free–free Euler beam.

F_{pn} in Eq. (7) represents the restoring force in the nth pad, given by

$$F_{pn} = K_p[U_r(z_{pn}) - U_{sn}] = \frac{K_p(K_b - m_s\omega^2)}{K_p - m_s\omega^2 + K_b} U_r(z_{pn}), \quad n = 1, 2, \ldots, N. \tag{10}$$

Both F_{1m} and F_{1hj} in Eqs. (7) and (8), respectively, represent the restoring force between the rail and bottom mass-bar of the hth absorber, but the former is in the global coordinates of the rail, and the latter is in the local coordinates of the hth absorber. When $m = (h-1) \times M_p + j$, z_m and z_{hj} indicate the same position, and thus F_{1m} and F_{1hj} are a pair of action and reaction force and given by

$$F_{1m} = K_1[U_r(z_m) - U_{1h}(z_{hj})] = -F_{1hj}, \quad h = 1, 2, \ldots, M_a, \ j = 1, 2, \ldots, M_p. \tag{11}$$

Similar situation happens to F_{3m} and F_{3hj} in Eqs. (7) and (9), which represent the restoring force between the rail and upper mass-bar of the hth absorber. F_{3m} and F_{3hj} are the action and reaction force pair when $m = (h-1) \times M_p + j$, given as

$$F_{3m} = K_3[U_r(z_m) - U_{2h}(z_{hj})] = -F_{3hj}, \quad h = 1, 2, \ldots, M_a, \ j = 1, 2, \ldots, M_p. \tag{12}$$

F_{2hj} in Eqs. (8) and (9) represent the jth restoring force between upper and bottom mass-bars in the hth absorber, given as

$$F_{2hj} = K_2[U_{2h}(z_{hj}) - U_{1h}(z_{hj})], \quad h = 1, 2, \ldots, M_a, \ j = 1, 2, \ldots, M_p. \tag{13}$$

From Eq. (7) the rail displacement at the specific point z_{pi} and z_l, the pad position and the connecting point to the absorber, respectively, can be represented by

$$U_r(z_{pi}) = F\alpha(z_{pi}, 0) - \sum_{n=1}^{N} F_{pn}\alpha(z_{pi}, z_{pn}) - \sum_{m=1}^{M}(F_{1m} + F_{3m})\alpha(z_{pi}, z_m), \quad i = 1, 2, \ldots, N, \tag{14}$$

$$U_r(z_l) = F\alpha(z_l, 0) - \sum_{n=1}^{N} F_{pn}\alpha(z_l, z_{pn}) - \sum_{m=1}^{M}(F_{1m} + F_{3m})\alpha(z_l, z_m), \quad l = 1, 2, \ldots, M. \tag{15}$$

From Eqs. (8) and (9) the displacement of the bottom and upper mass-bar of the hth absorber at z_{hk}, the connecting position to the rail in the local coordinates, can be given by

$$U_{1h}(z_{hk}) = -\sum_{j=1}^{M_p}(F_{1hj} - F_{2hj})\beta_1(z_{hk}, z_{hj}), \quad h = 1, 2, \ldots, M_a, \ \ k = 1, 2, \ldots, M_p, \tag{16}$$

$$U_{2h}(z_{hk}) = -\sum_{j=1}^{M_p}(F_{2hj} + F_{3hj})\beta_2(z_{hk}, z_{hj}), \quad h = 1, 2, \ldots, M_a, \ \ k = 1, 2, \ldots, M_p. \tag{17}$$

Substituting Eqs. (14)–(17) for the rail and absorber displacement in Eqs. (10)–(13) leads to

$$F_{pi}\frac{K_p - m_s\omega^2 + K_b}{K_p(K_b - m_s\omega^2)} + \sum_{n=1}^{N} F_{pn}\alpha(z_{pi}, z_n) + \sum_{m=1}^{M}(F_{1m} + F_{3m})\alpha(z_{pi}, z_m) = F\alpha(z_{pi}, 0),$$
$$i = 1, 2, \ldots, N, \tag{18}$$

$$\frac{F_{1l}}{K_1} + \sum_{n=1}^{N} F_{pn}\alpha(z_l, z_n) + \sum_{m=1}^{M}(F_{1m} + F_{3m})\alpha(z_l, z_m) - \sum_{j=1}^{M_p}(F_{1hj} - F_{2hj})\beta_1(z_{hk}, z_{hj}) = F\alpha(z_l, 0),$$
$$l = 1, 2, \ldots, M, \ \ h = 1, 2, \ldots, M_a, \ \ k = 1, 2, \ldots, M_p \quad \text{for } \ l = (h-1) \times M_p + k, \tag{19}$$

$$\frac{F_{3l}}{K_3} + \sum_{n=1}^{N} F_{pn}\alpha(z_l, z_n) + \sum_{m=1}^{M}(F_{1m} + F_{3m})\alpha(z_l, z_m) - \sum_{j=1}^{M_p}(F_{2hj} + F_{3hj})\beta_2(z_{hk}, z_{hj}) = F\alpha(z_l, 0),$$
$$l = 1, 2, \ldots, M, \ \ h = 1, 2, \ldots, M_a, \ \ k = 1, 2, \ldots, M_p \quad \text{for } \ l = (h-1) \times M_p + k, \tag{20}$$

$$\frac{F_{2hk}}{K_2} + \sum_{j=1}^{M_p}(F_{2hj} + F_{3hj})\beta_2(z_{hk}, z_{hj}) - \sum_{j=1}^{M_p}(F_{1hj} - F_{2hj})\beta_1(z_{hk}, z_{hj}) = 0, \quad h = 1, 2, \ldots, M_a, \ \ k = 1, 2, \ldots, M_p. \tag{21}$$

Combine Eqs. (18)–(21) to form a matrix equation as

$$\mathbf{AF} = \mathbf{B}, \tag{22}$$

where $\mathbf{A}$ is a square matrix with its elements composed by the rail and absorber receptance, α, β_1 and β_2, and other receptance terms, $(K_p - m_s\omega^2 + K_b)/[K_p(K_b - m_s\omega^2)]$, $1/K_1$, $1/K_2$ and $1/K_3$, $\mathbf{F}$ is the unknown force vector that consists of the restoring forces in the rail pads and absorbers, and $\mathbf{B}$ is a vector composed of $F\alpha(z_i, 0)$ and zero elements.

By solving Eq. (22), the restoring forces in the pad and absorber are obtained. Substituting the forces into Eqs. (7)–(9), the amplitude of vibration of the rail and absorber are known.

3. Parameters of rail absorber and basic results

The effectiveness of the rail absorber is related to the tuned frequency, active mass and damping parameters of the absorber. In Ref. [7] the first and second resonance frequency of rigid body motion of the absorber is designed to be 250 and 700 Hz, respectively. At the second resonance, the bottom mass-bar of the absorber oscillates with large amplitude and out of phase with the upper mass-bar, whereas the vibration amplitude of the upper mass-bar is small, even smaller than the rail. The rail vibration energy dissipates through the deformation of the elastomeric layers of the absorber, which is mainly caused by the vibrating motion of the bottom mass-bar. Therefore, the absorber's second resonance frequency of rigid body motion should be designed to be close to that at which the rail vibration and radiation are maximum. Predictions of rolling noise

from the TWINS models (Track–Wheel Interaction Noise Software) showed that the main component of rolling noise is from rail radiation, with its peak being at about 650–850 Hz for a train speed 100 km/h and a roughness spectrum corresponding to tread-braked wheels on a smooth rail [8].

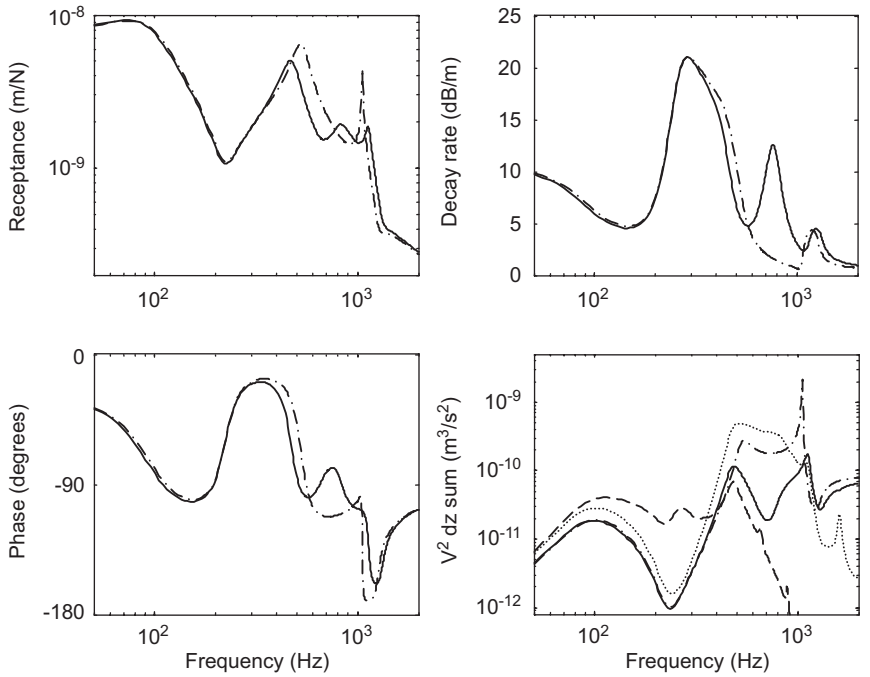

Fig. 3. Vibration receptance, decay rate and energy due to a unit excitation at mid-span (quarter of absorber): — rail with absorber, –·– rail without absorber, –– upper mass-bar of absorber, · · · · · · bottom mass-bar of absorber.

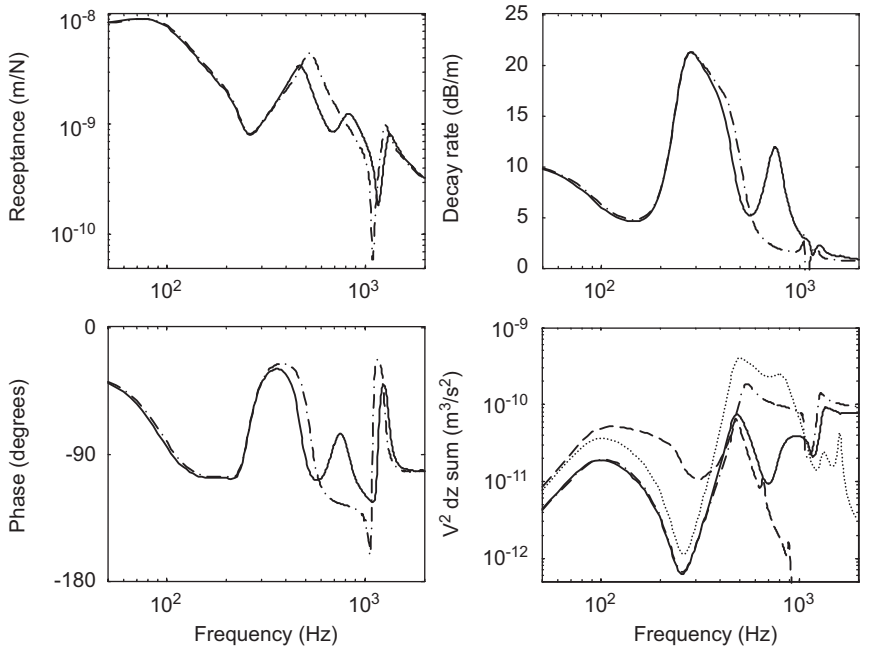

Fig. 4. Vibration receptance, decay rate and energy due to a unit excitation above a sleeper (middle of absorber), keys as for Fig. 3.

Table 1
Natural frequency of 1.2 m long absorber.

Mode	1	2	3	4	5	6	7
Frequency, Hz	247	342	472	656	697	734	881
Mode	8	9	10	11	12	13	14
Frequency, Hz	887	1155	1166	1507	1580	1859	2106

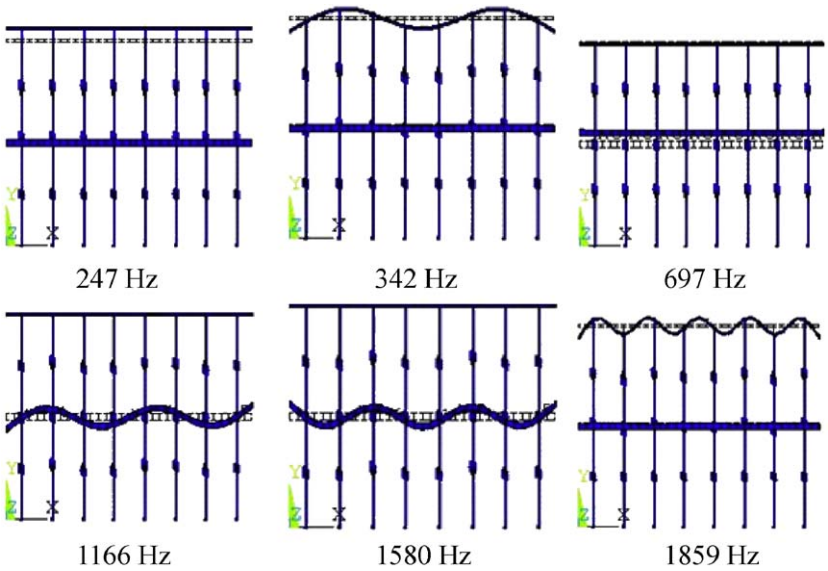

Fig. 5. Selected vibration mode-shapes of 1.2 m long absorber.

The resonance frequency of the absorber is determined by both the mass and the stiffness of the elastomeric layers of the absorber. Large active mass is helpful to enhance the effectiveness of the absorber, but confined by the size of the rail cross-section. The absorber damping is important for rail vibration attenuation. Both over high and over low loss factor of the damping material used in the absorber may degrade its effectiveness.

In Ref. [7] the optimal parameters were obtained for the rail absorber after extensive parametric studies. They are transformed and used here for the double-beam model of the absorber and given as

$$EI_1 = 2.8 \times 10^4\,\mathrm{N\,m^2}, \quad EI_2 = 2.1 \times 10^3\,\mathrm{N\,m^2}, \quad \rho A_1 = 14\,\mathrm{kg/m}, \quad \rho A_2 = 6\,\mathrm{kg/m},$$
$$K_1 = 39\,\mathrm{MN/m}, \quad K_2 = 1.8\,\mathrm{MN/m}, \quad K_3 = K_2/4, \quad \eta_a = 0.25, \quad L_a = 1.2\,\mathrm{m}, \quad d = 0.15\,\mathrm{m},$$

where L_a is the length of rail absorber.

UIC60 rail is chosen for calculation and the parameters are

$$E = 2.1 \times 10^{11}\,\mathrm{N/m^2}, \quad G = 0.77 \times 10^{11}\,\mathrm{N/m^2}, \quad \eta_r = 0.01, \quad k = 0.4,$$
$$\rho = 7850\,\mathrm{kg/m^3}, \quad A_r = 7.69 \times 10^{-3}\,\mathrm{m^2}, \quad I_r = 30.55 \times 10^{-6}\,\mathrm{m^4},$$

where η_r is the loss factor of the rail.

The parameters for the discrete supports are

$$K_p = 350\,\mathrm{MN/m}, \quad \eta_p = 0.2, \quad K_b = 50\,\mathrm{MN/m}, \quad \eta_p = 1.0, \quad m_s = 162\,\mathrm{kg}, \quad D = 0.6\,\mathrm{m}.$$

The dynamic behaviour of the rail with the 1.2 m long absorber is shown in Figs. 3 and 4 for a unit harmonic force applied at mid-span and above a sleeper, respectively, in terms of the point receptance and decay

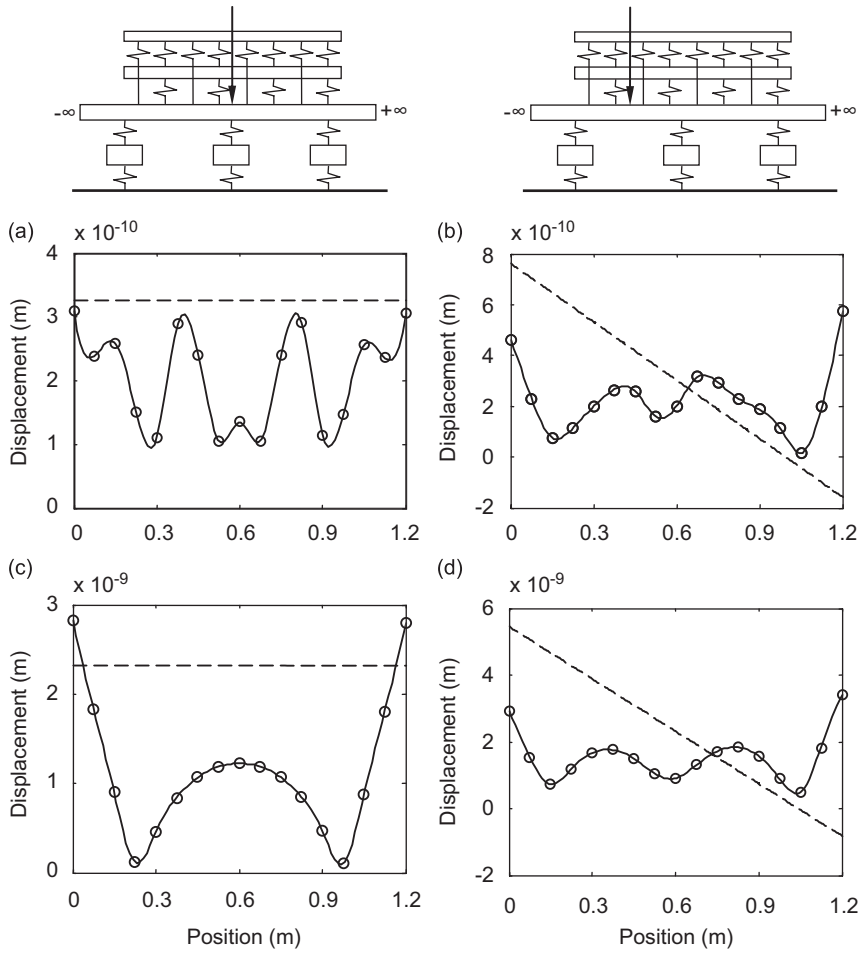

Fig. 6. Vibration displacement of 1.2 m long absorber at 697 Hz due to a unit excitation above a sleeper and at mid-span: –o– bending deformation, –– rigid body motion; (a) and (b) for upper mass-bar, (c) and (d) for bottom mass-bar.

rate of rail vibration and the vibration energy level of the rail, bottom and upper mass-bar of the absorber. The decay rate is estimated through attenuation in the rail vibration amplitude between the forcing point and another point over five sleeper spans apart divided by the distance between them. The vibration energy is evaluated by sum $|v|^2\,\mathrm{d}z$, where v is the amplitude of vibration velocity and $\mathrm{d}z$ is the length of a small track section.

It can be seen from Figs. 3 and 4 that three resonances in the receptance are at about 80, 500 and 1100 Hz, corresponding to the whole track bounces on the ballast, the rail vibrates on the pad and the 'pinned–pinned' resonance of track vibration, respectively. The pinned–pinned resonance peak can be seen to be suppressed by the rail absorber.

The decay rate of rail vibration with and without the absorber can be seen to reach a peak about 20 dB/m at 300 Hz. When the rail absorber is used, the decay rate of rail vibration is significantly increased in the frequency region 600–1100 Hz, and thus the rail vibration energy is substantially reduced in this frequency region. As the pinned–pinned resonance is suppressed by the absorber, so is the peak in the rail vibration energy at the corresponding frequency for the force applied at mid-span of a sleeper bay.

From Figs. 3 and 4 the energy level of the upper mass-bar of the absorber can be seen to be higher than that of the rail up to about 300 Hz, but lower at higher frequencies. Around the second resonance frequency of the absorber it can be seen that the vibration energy of the bottom mass-bar is much higher than that of the rail.

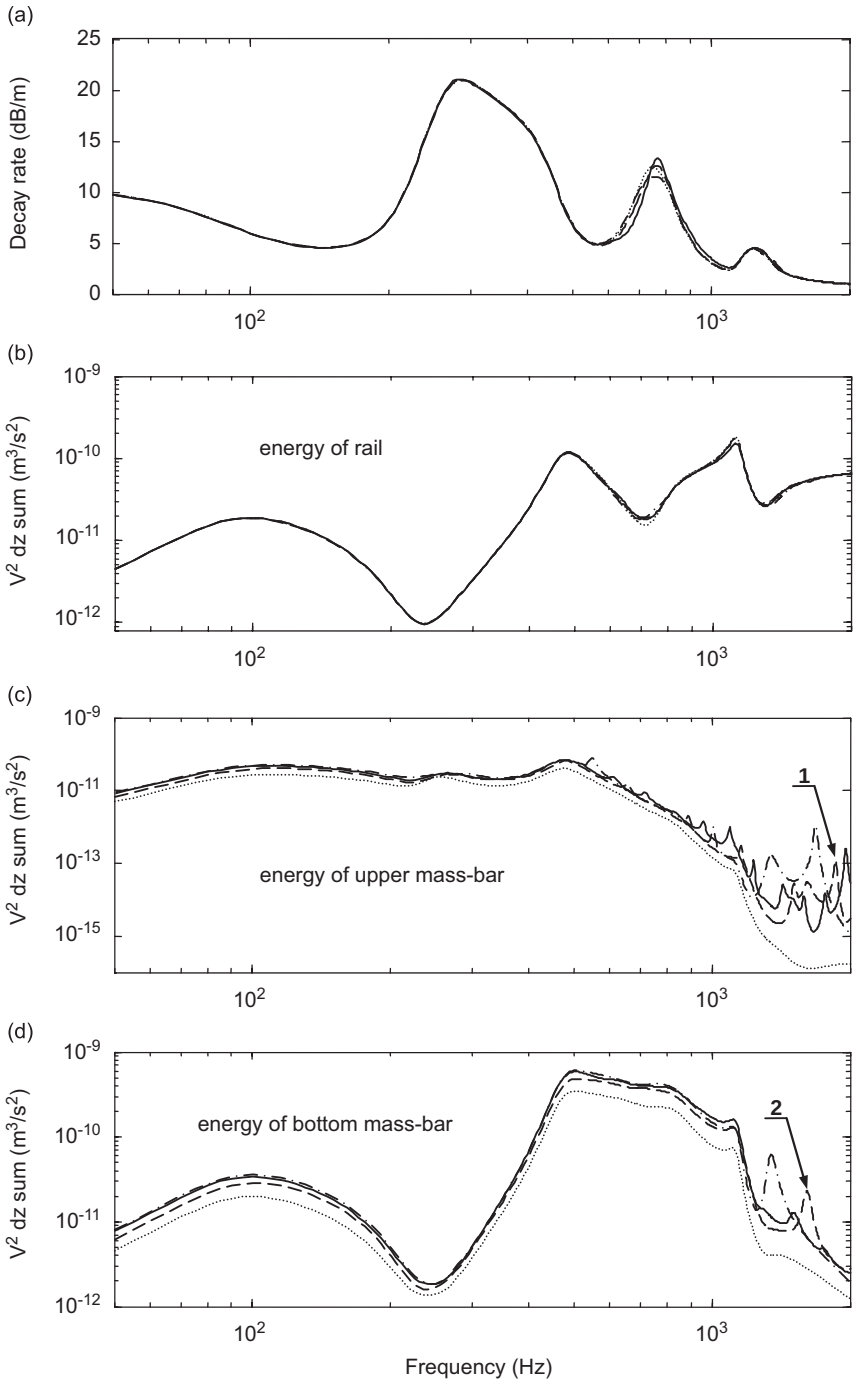

Fig. 7. Vibration decay rate and energy of rail with absorber in different length due to a unit excitation at mid-span: · · · · · · from mass–spring absorber model, –·– 0.6 m long absorber, –– 1.2 m long absorber, — 2.4 m long absorber.

This indicates large amplitude of vibration of the bottom mass-bar, which leads to large deformation of the elastomeric layers of the absorber and dissipation of the rail vibration energy. At high frequencies a couple of peaks in the vibration energy of the absorber can be observed. They are associated with the bending modes of the mass-bars of the absorber. This will be further discussed in the next section.

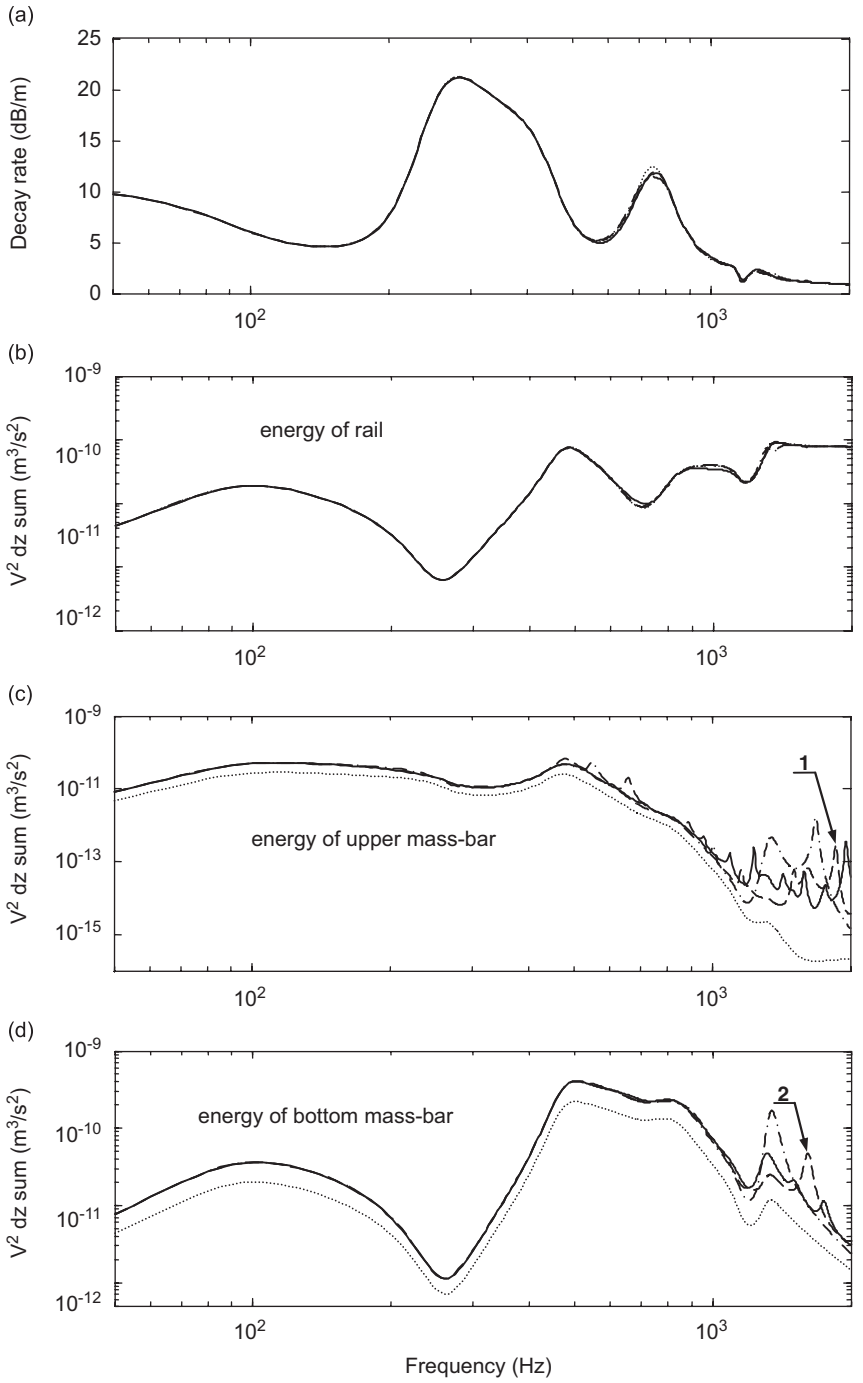

Fig. 8. Vibration decay rate and energy of rail with absorber in different length due to a unit excitation above a sleeper, keys as for Fig. 7.

4. Parametric study of effectiveness of rail absorber

In this section parametric studies are conducted to investigate the influences of the bending modes of the rail absorber on its effectiveness. Apart from the material parameters, the bending modes of the rail absorber are determined by its geometric parameters, i.e. the length and the cross-sectional area moment of inertia, provided that the mass per unit length keeps unchanged for the absorber.

Table 2
Cross-sectional parameters of rail absorber on one side of the rail web.

Case	A_1 = width × height, m^2	I_1, $10^{-8}\,m^4$	A_2 = width × height, m^2	I_2, $10^{-8}\,m^4$
1	0.033 × 0.027	5.4	0.03 × 0.0127	0.5
2	0.03 × 0.03	6.7	0.03 × 0.0127	0.5
3	0.0225 × 0.04	12	0.03 × 0.0127	0.5
4	0.03 × 0.03	6.7	0.033 × 0.012	0.4
5	0.03 × 0.03	6.7	0.03 × 0.0127	0.5
6	0.03 × 0.03	6.7	0.017 × 0.023	1.7

4.1. Vibration modes of absorber

The vibration modes of the absorber are calculated using ANSYS codes. The absorber is modelled as a double beam–spring system attached to the rail with free–free boundary conditions applied to the beams, and the rail is fixed when calculating the vibration modes of the absorber. The natural frequencies of the 1.2 m long absorber are listed in Table 1, and six selected vibration modes of the absorber are shown in Fig. 5. The first and fifth modes at 247 and 697 Hz, respectively, are rigid body motion of the absorber. In the first mode of rigid body motion the upper mass-bar oscillates up and down, while in the second one the bottom mass-bar oscillates. The other modes are bending modes of the absorber.

The vibration response of the absorber attached to the rail includes rigid body motion and bending deformation. Fig. 6 shows the motion and deformation components of the 1.2 m long absorber when a harmonic excitation is applied to the rail above a sleeper and at mid-span of a sleeper bay. The two forcing places are relatively in the middle and quarter of the absorber. It can be observed that the rigid body motion is dominant in the vibration response of the absorber. This implies that the decay of rail vibration and dissipation of the vibration energy are mainly associated with the rigid body motion of the absorber. In other words, the influences of the bending modes are expected to be a secondary matter on the effectiveness of the rail absorber. The following parametric studies will validate the above inference.

4.2. Influences of absorber length

The vibration modes of the rail absorber are associated with its length. A long beam shows lower natural frequencies and more vibration modes within a certain frequency range, compared with a short beam. Figs. 7 and 8 show the calculation results from the absorber with different lengths 0.6, 1.2, and 2.4 m for a unit excitation applied at mid-span and above a sleeper, respectively, in terms of the decay rate of rail vibration and vibration energy of the rail and absorber. Also shown in Figs. 7 and 8 are the results from the mass–spring model of the absorber for comparison.

The decay rate of rail vibration can be seen from Figs. 7 and 8 to be very similar among the different absorbers. The rail vibration energy is almost the same for the absorbers with different lengths. However, differences can be found in the vibration energy of the absorbers. For the mass–spring absorber model the vibration energy of the absorber varies smoothly, whereas for the beam model many peaks in the vibration energy can be observed due to the bending modes of beam vibration. For instance, the vibration energy peaks pointed with 1 and 2 in Figs. 7 and 8 are associated with the bending modes of the absorber at 1580 and 1859 Hz, respectively. Anyway, the energy peaks due to the bending modes will not degrade the performance of the absorber, because the vibration level of the upper mass-bar of the absorber is much lower than that of the rail, and large amplitude of vibration of the bottom mass-bar is helpful to the energy dissipation of rail vibration.

4.3. Influences of inertia moment of cross-sectional area

Provided the cross-sectional area keeps unchanged, the area moment of inertia can be adjusted by altering the width and height of the cross-section of the rail absorber, and thus the bending modes of the absorber is also adjusted. To investigate the influences on the effectiveness of the rail absorber due to change of the area moment of

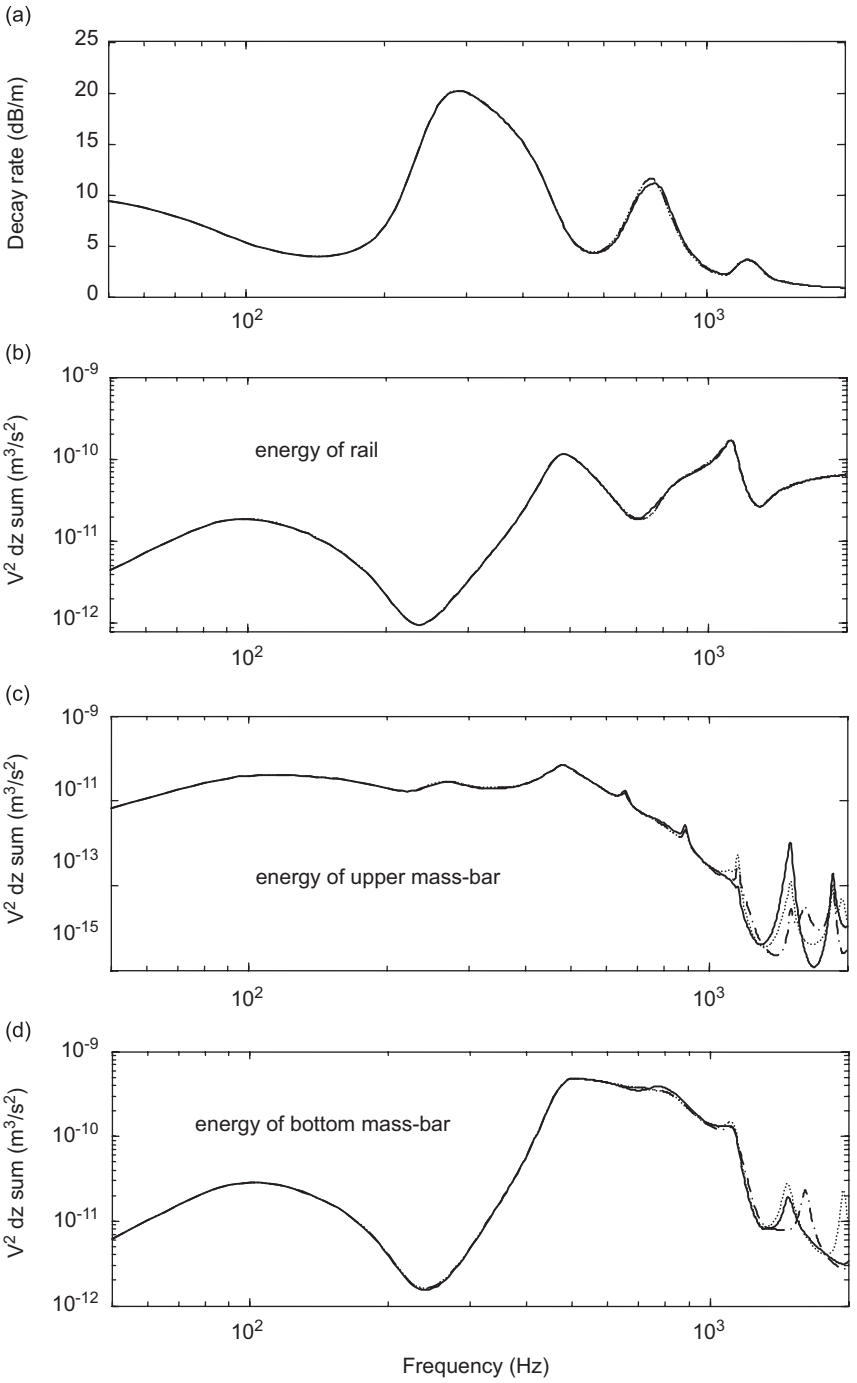

Fig. 9. Vibration decay rate and energy of rail with absorber due to a unit excitation at mid-span for different cross-sectional parameters of bottom mass-bar: · · · · · · case 1, – · – case 2, — case 3.

inertia, six cases are considered in the calculations, in which the cross-sectional area keeps unchanged but the area moment of inertia is adjusted for the absorber. The cross-section parameters of the absorber used for the six calculation cases are listed in Table 2. In the first three cases the cross-sectional area moment keeps unchanged for the upper mass-bar, whereas in the last three cases it keeps unchanged for the bottom mass-bar. The calculation results of the six cases for the 1.2 m long absorber are shown in Figs. 9 and 10 due to a unit excitation applied at mid-span.

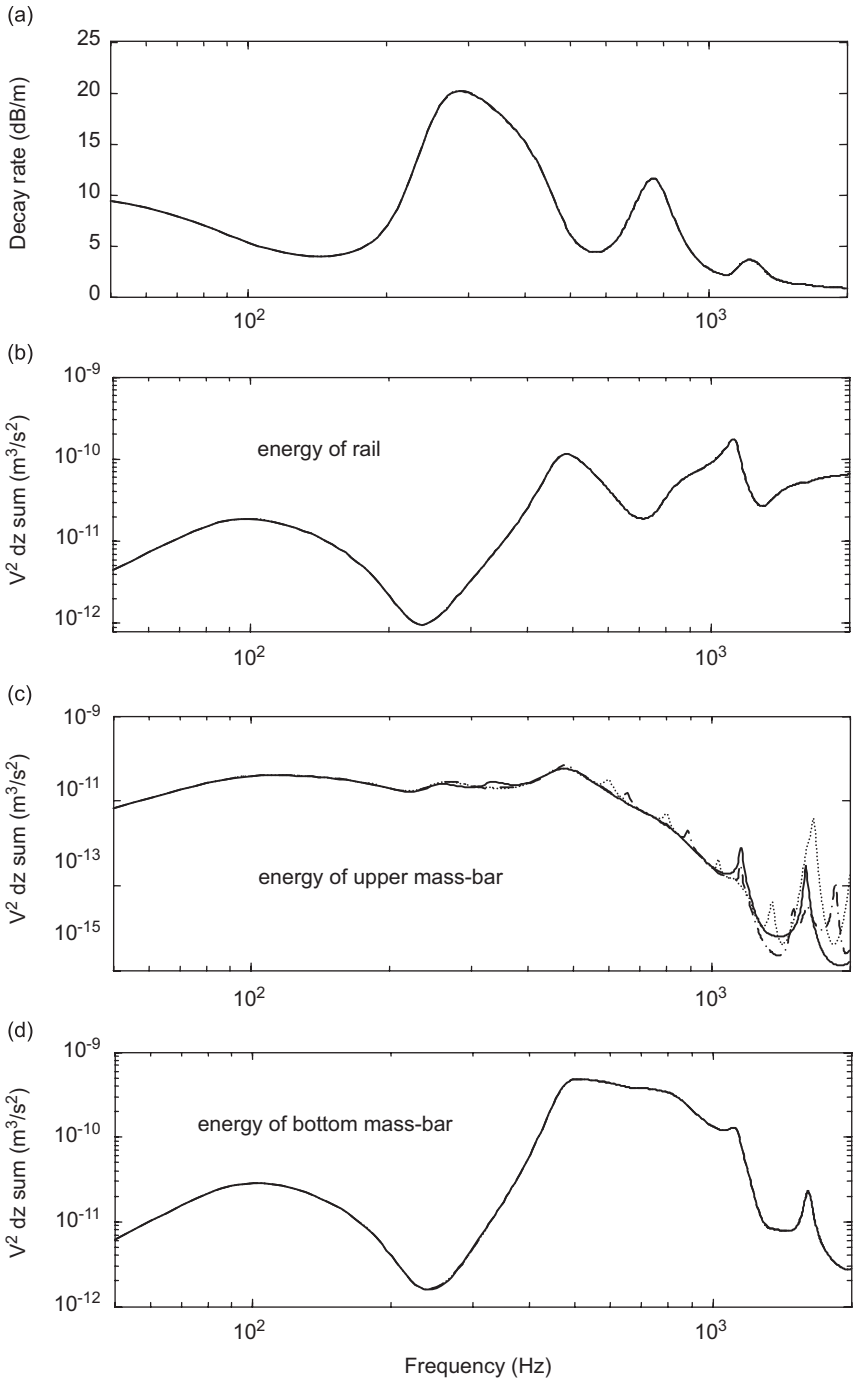

Fig. 10. Vibration decay rate and energy of rail with absorber due to a unit excitation at mid-span for different cross-sectional parameters of upper mass-bar: · · · · · · case 4, –·– case 5, — case 6.

In Figs. 9 and 10 the decay rate and energy level of rail vibration are shown to be almost the same for the six cases when changing the cross-sectional area moment of the absorber, although the vibration energy level of the absorber varies with the area moment of inertia. This means that the performance the rail absorber will not be affected by its cross-section size, provided that the mass per unit length keeps unchanged for the absorber.

5. Conclusions

A compound track model with the rail absorber is developed, in which the rail is represented by an infinite Timoshenko beam and the absorber is modelled as a damped beam–spring system attached to the rail. Using this model the dynamic behaviour of the track and the effectiveness of the absorber are studied and compared with those from an untreated track. The influences of the bending modes of the rail absorber on its performance are investigated.

The calculation results show that the decay rate of rail vibration is significantly increased in the frequency region of 600–1100 Hz and the pinned–pinned resonance of track vibration is suppressed by use of the rail absorber. The rail vibration energy is therefore substantially reduced in the corresponding frequency region, and thus the rail radiated noise can effectively be reduced. As the rigid body motion is dominant in the vibration response of the absorber, it is the main cause that leads to energy dissipation of rail vibration, whilst the effects of the bending deformation of the absorber are secondary and slight. Therefore it can be concluded that a simple mass–spring model is enough to represent the rail absorber instead of an advanced beam–spring model.

Acknowledgements

This study has been carried out under the Action Programme supported by the Ministry of Science and Technology of the People's Republic of China, Grant No. 2008BAQG0010.

Appendix A

The equation of motion for the finite Euler–Bernoulli beam with a unit harmonic load applied at $z = z_1$ is given by

$$\rho A \frac{\partial^2 u}{\partial t^2} + EI(1 + i\eta)\frac{\partial^4 u}{\partial z^4} = e^{i\omega t}\delta(z - z_1). \tag{A.1}$$

The steady response of the beam can be given in the form of modes superposition

$$u(z, t) = U(z)e^{i\omega t} = \sum_{n=1}^{N} W_n(z)q_n(t), \tag{A.2}$$

where $W_n(z)$ is the nth normalized mode-shape function, $q_n(t)$ is the nth modal coordinate, and N is the number of the modes considered. For the free–free beam $W_n(z)$ is given by

$$\begin{cases} W_1(z) = \dfrac{1}{\sqrt{\rho AL}}, & \\ W_2(z) = \dfrac{1}{\sqrt{\rho AL}}\sqrt{3}(1 - 2z/L), & 0 \leqslant z \leqslant L, \\ W_n(z) = \dfrac{1}{\sqrt{\rho AL}}[(\cosh k_n z + \cos k_n z) + c_n(\sinh k_n z + \sin k_n z)], & n \geqslant 3, \end{cases} \tag{A.3}$$

where parameters k_n and c_n are listed in Table 3. The first and second mode-shape functions are for the rigid body motion, and the third and subsequent ones are for the bending modes. The orthogonal integrals for

Table 3
Parameters of the mode-shape function of free–free beam.

Mode n	1	2	3	4	5	$\geqslant 6$
c_n	–	–	0.9825	1.0008	1.0000	1.0000
k_nL	0	0	4.7300	7.8532	10.996	$(2n-3)\pi/2$

$W_n(z)$ are given as follows [9]:

$$\int_0^L \rho A W_m(z) W_n(z)\,\mathrm{d}z = \begin{cases} 1, & m = n, \\ 0, & m \neq n. \end{cases} \tag{A.4}$$

Substituting Eq. (A.2) into Eq. (A.1) gives

$$\rho A \sum_{n=1}^{N} W_n(z)\ddot{q}_n(t) + EI(1+i\eta)\sum_{n=1}^{N} W_n''''(z) q_n(t) = \mathrm{e}^{\mathrm{i}\omega t}\delta(z - z_1). \tag{A.5}$$

Multiplying Eq. (A.5) by $W_m(z)$ and performing integration on both side from $z = 0$ to $z = L$ yields

$$\ddot{q}_n(t) + \frac{EI(1+\mathrm{i}\eta)}{\rho A} k_n^4 q_n(t) = W_n(z_1)\mathrm{e}^{\mathrm{i}\omega t}. \tag{A.6}$$

Solving Eq. (A.6) for $q_n(t)$ results in

$$q_n(t) = \frac{W_n(z_1)}{\omega_n^2 - \omega^2 + \mathrm{i}\eta\omega_n^2}\mathrm{e}^{\mathrm{i}\omega t}, \tag{A.7}$$

where $\omega_n = k_n^2\sqrt{(EI/\rho A)}$ is the natural frequency of the nth vibration mode of the free–free beam.

Substituting Eq. (A.7) into Eq. (A.2), the displacement amplitude of the free–free beam due to the unit harmonic force is obtained as

$$U(z) = \sum_{n=1}^{N} \frac{W_n(z) W_n(z_1)}{\omega_n^2 - \omega^2 + \mathrm{i}\eta\omega_n^2}. \tag{A.8}$$

Setting $z = z_2$ in Eq. (A.8), the transfer receptance of the free–free beam is given by

$$\beta(z_2, z_1) = \sum_{n=1}^{N} \frac{W_n(z_2) W_n(z_1)}{\omega_n^2 - \omega^2 + \mathrm{i}\eta\omega_n^2}. \tag{A.9}$$

References

[1] P.J. Remington, Wheel/rail noise I: characterization of the wheel/rail dynamic system, *Journal of Sound and Vibration* 46 (1976) 359–379.

[2] D.J. Thompson, Wheel–rail noise generation, part I: introduction and interaction model, *Journal of Sound and Vibration* 161 (1993) 387–400.

[3] D.J. Thompson, Wheel–rail noise generation, part II: wheel vibration, *Journal of Sound and Vibration* 161 (1993) 401–419.

[4] D.J. Thompson, Wheel–rail noise generation, part III: rail vibration, *Journal of Sound and Vibration* 161 (1993) 421–446.

[5] T.X. Wu, D.J. Thompson, A double Timoshenko beam model for vertical vibration analysis of railway track at high frequencies, *Journal of Sound and Vibration* 224 (1999) 329–348.

[6] D.J. Thompson, C.J.C. Jones, T.P. Waters, D. Farrington, A tuned damping device for reducing noise from railway track, *Applied Acoustics* 68 (2007) 43–57.

[7] T.X. Wu, On the railway track dynamics with rail vibration absorber for noise reduction, *Journal of Sound and Vibration* 309 (2008) 739–755.

[8] D.J. Thompson, C.J.C. Jones, T.X. Wu, G. de France, The influence of the non-linear stiffness behaviour of rail pads on the track component of rolling noise, *Proceedings of the IMechE Part F: Journal of Rail and Rapid Transit* 213 (1999) 233–241.

[9] C.W. De Silve, *Vibration and Shock Handbook*, CRC Press, Boca Raton, FL, 2005.